Solar Energy Materials & Solar Cells 137 (2015) 44–49

Contents lists available at ScienceDirect

Solar Energy Materials & Solar Cells

journal homepage: www.elsevier.com/locate/solmat

Enhanced stability in semi-transparent PTB7/PC71BM photovoltaic cells

Pablo Romero-Gomez [a,*], Rafael Betancur [a], Alberto Martinez-Otero [a], Xavier Elias [a], Marina Mariano [a], Beatriz Romero [b], Belén Arredondo [b], Ricardo Vergaz [c], Jordi Martorell [a,d]

[a] ICFO-Institut de CienciesFotoniques, Mediterranean Technology Park, 08860 Castelldefels, Barcelona, Spain
[b] Escuela de Ciencias Experimentales y Tecnología, Universidad Rey Juan Carlos, 28933 Móstoles, Madrid, Spain
[c] Escuela Politécnica Superior, Universidad Carlos III de Madrid, 28911 Leganés, Madrid, Spain
[d] Departament de Fisica i Enginyeria Nuclear, Universitat Politècnica de Catalunya, Terrassa, Spain

ARTICLE INFO

Article history:
Received 5 September 2014
Received in revised form
1 January 2015
Accepted 18 January 2015
Available online 7 February 2015

Keywords:
PTB7
OSC
Stability
Warburg
Inverted
Photonic crystal

ABSTRACT

We studied the performance over time of opaque and semi-transparent PTB7:PC71BM bulk heterojunction solar cells. For unsealed inverted configuration cells we observe that when the isolation from the environment is improved, the degradation observed is dominated by one single exponential decay. We demonstrate that a dielectric multilayer stack of approximately 550 nm provides an isolation that increases the lifetime of the cell close to ten times. In that event the fill factor appears to be the PV parameter dominating cell degradation resulting from a decrease in the shunt resistance. An Impedance analysis we performed indicates that a Warburg element, attributed to the presence of slowly moving charges such as heavy ions, must be included in the description of the experimental data. The contribution from such element increases as the cell degrades in good agreement with a degradation dominated by the corrosive effects from external agents reaching the active layer of the device.

1. Introduction

Since the early works on organic solar cells (OSC), many different polymers have been synthesized towards the goal of obtaining an active material with an optimal photon to charge conversion that would make such type of cells a commercially viable technology. In recent years, cells made with bulk hetero-junctions (BHJ) of PTB7/$PC_{71}BM$ have emerged as one of the most promising polymer based devices combining the unique features of an organic based technology with a relatively high power conversion efficiency (PCE) [1,2]. Interestingly, it has been shown that such polymer blend can be used to obtain high performance homogenously semi-transparent solar cells [3]. Unlike semi-transparent cells fabricated using other types of polymers or PV technologies, with PTB7 one may fabricate devices which do not alter the colour of the objects seen through them. However, despite the high PCEs obtained and the potential for the PTB7/$PC_{71}BM$ blend to be used in building integrated PV, any practical application for such cells would be pending on the final stability of the devices fabricated using such blend.

For many different kinds of organic based PV cells it has been reported that the penetration of oxygen and moisture into the active layer of the cell results in severe loss of performance [4–8]. In the standard OPV configuration, the acidic nature of the poly(3,4-ethylenedioxylenethiophene):poly(styrenesulphonic acid) (PEDOT:PSS) used as electron blocking layer (EBL) [9,10] leads the etching of the indium tin oxide (ITO) electrode [11]. For instance, in P3HT oxygen has been demonstrated to react with the side chain by insertion in the alpha position relative to the thiophene ring [12]. In polyfluorenes oxygen insertion next to the quaternary carbon leads to fluorenone units and results in severe damage of the polymer properties [13]. Blocking of similar carbon positions with bulky side chains that prevent oxygen insertion has resulted in important increases in device stability [14], especially when aryl groups are used instead of alkyl chains. Large improvements in the stability of organic devices can be obtained in inverted configurations that bypass the need to use PEDOT:PSS. In such architecture, n-type metal oxides such as ZnO or TiO_2 are deposited on the ITO layer to lower the work function of the electrode [15,16], while NiO, WO_3 or MoO_3 may be used as EBL [11]. Further improvements in stability may be reached by an adequate isolation from the most aggressive external agents [4].

In the current work we study the stability of cells which use PTB7:PC71BM as the active blend. In particular we show that the

* Corresponding author.
E-mail address: pablo.romero@icfo.es (P. Romero-Gomez).

http://dx.doi.org/10.1016/j.solmat.2015.01.026
0927-0248/

incorporation of a 1-D multilayer structure combining three layers of high refractive index (HRI) and two layers of low refractive index (LRI) dielectric materials to enhance the efficiency of semi-transparent cells [3] acts also as an efficient barrier to protect the cell from a rapid degradation. In the first part of the work, a comparison between the stability of opaque and semi-transparent cells is provided. In the second, the performance of opaque and semi-transparent inverted devices is compared, and the impact of the multilayer structure (ML) over the long term stability is analysed.

2. Experimental

2.1. Device fabrication

To fabricate the photovoltaic devices we used 120 nm thick ITO-patterned substrates. For the standard configuration, PEDOT:PSS was used as EBL while thermally evaporated BCP as HBL. Details of the preparation of such cells can be found elsewhere [17]. For the inverted solar cells, a thermally evaporated MoO_3 layer was used as EBL while ZnO was used as HBL. The ZnO layer was grown by sol–gel where the precursor solution was prepared according to Ref [18]. Spin coating was performed at 6000 rpm during 60 s followed by a thermal annealing at 200 °C during 20 min in air. In the semi-transparent devices, a 10 nm thick silver back electrode was thermally evaporated at 5.5 Å s^{-1} onto a substrate cooled down to −5 °C [19]. The thicknesses for all the layers are reported in Table 1 (note that all devices have the same active layer thickness). We fabricated five different types of non-encapsulated PTB7:$PC_{71}BM$ BHJ cell architectures (see Fig. 1): Standard opaque (Std-Opaque), Standard semi-transparent (Std-ST), inverted opaque (Inv-Opaque), inverted semi-transparent (Inv-ST), and inverted semi-transparent with a multilayer trapping structure (Inv-ML-ST). Thicknesses of the photovoltaic cell layers were determined numerically to optimize light harvesting in the opaque configuration [3,17,20] with the only constraints imposed by the fabrication procedures or the charge collection limitations of the materials used. The photovoltaic part and the photonic structure deposited on top of the transparent Ag electrode may be clearly distinguished in the field-emission scanning electron microscopy (FESEM) cross-section view of the Inv-ML-ST device shown in Fig. 2.

In order to make Std-ST, Inv-ST, and Inv-ML-ST devices semi-transparent, the back silver contact was made 10 times thinner than for the opaque cells (i.e. 10 nm instead of 100 nm thickness). Std-ST and Inv-ST devices where capped with a 10 nm protective MoO_3 layer deposited on top of the back Ag contact. For the Inv-ML-ST device, such protective layer was replaced by the photonic crystal, a five-layer structure based on MoO_3 (HRI) and MgF_2 (LRI). The structure was designed numerically to provide the adequate light management to optimize the performance of the cell, i.e. to increase light trapping in the near IR and near UV region. Details on such numerically based optical optimization for semi-transparent cells can be found in Ref. [3], where a similar analysis was applied to optimize the PCE of semi-transparent standard cells.

Table 1
Thicknesses (in nm) for all layers in the five different configurations considered.

	ITO	PEDOT:PSS	ZnO	BHJ	BCP	MoO_3	Ag	MoO_3/MgF_2
Std-Opaque	120	40	–	100	3.5	–	100	–
Std-ST	120	40	–	100	3.5	–	10	10/0/0/0/0
Inv-Opaque	120	–	30	100	–	5	100	–
Inv-ST	120	–	30	100	–	5	10	10/0/0/0/0
Inv-ML-ST	120	–	30	100	–	5	10	112/136/102/102/102

2.2. Device characterization

The PCE of the fabricated devices was determined from current density–voltage curve measurements obtained under 1 sun, AM 1.5G spectrum illumination from a solar simulator (Abet Technologies, model Sun 3000). The solar simulator illumination intensity was monitored using a monocrystal silicon reference cell (Rera Systems) calibrated against a National Renewable Energy Laboratory calibrated reference cell. In the characterization of all semi-transparent cells, illumination was from the ITO side. Impedance spectroscopy (IS) measurements were performed under illumination conditions using a standard red LED. A Solartron 1260 impedance analyzer was used (Solartron Analytical, Farnborough, UK). The cell was connected to the analyzer that fed the input signal, biasing the device at different dc levels and superimposing an alternating signal with amplitude 100 mV and sweeping frequency from 1 Hz to 1 MHz.

3. Results and discussion

3.1. Time evolution of the PV parameters

The study the aging process of the fabricated devices was performed according to the ISOS-standards defined in Ref. [21]. We performed two sets of experiments. In one set we compared the performance of the Std-Opaque and Std-ST configurations relative to the Inv-Opaque one, while in a second set we compared the three different inverted configurations. The PV parameters for each cell were measured at the start of the aging process (cf. Table 2). All PV parameters measured subsequently were normalized to the corresponding initial values. In between measurements the cells were stored at ambient conditions in the dark, which corresponds to ISOS-D-1 shelf test at level 2 according to consensus stability testing protocols for OPVs [21]. With such level 2 test we aimed at determining the role played by the ML on the lifetime of the cells and determine the origin of cell degradation under such conditions. In our study, the cell lifetime is taken as the time the cell efficiency drops to 80% of its initial value [21].

The time evolution of the main PV parameters (V_{oc}, J_{sc}, FF and PCE) for the first set of time evolution experiments is shown in Fig. 3. As it has been reported with other polymer blends, the acidic nature of the PEDOT:PSS in contact with the ITO causes a rapid degradation of the FF and V_{oc} [22]. Such source of rapid degradation may mask any other source of degradation possibly related to the thickness of the capping metal electrodes and consequently we observe that Std-Opaque and Std-ST degrade at a very similar speed. On the contrary, the Inv-ST cells exhibit a lifetime of approximately 250 h, corresponding to at least 50 times the lifetime of the other two cells.

In the second set of experiments we considered only the inverse configurations. The evolution of all PV parameters for the three cells under study is shown in Fig. 4. As in the previous set of time evolution experiments the cells were stored in air and under darkness in between measurements. For all three inverted cells, the FF exhibits a degradation faster than V_{oc} and J_{sc}. Consequently the efficiency followed, to a large extent, the evolution of the FF. Note that the lifetime for the Inv-Opaque with a capping electrode of 100 nm is 800 h, close to three times the lifetime of the Inv-ST which is only capped with 10 nm of Ag and 10 nm of MoO_3. This suggests that external agents are a dominant source of degradation for the inverted cells and that thicker capping layer provide a better isolation from such agents. Note that for the Inv-ST and the Inv-Opaque a sudden drop in FF begins after 50 h and after 500 h, respectively. In the 3500 h of the study, this drop was not observed for the ML-ST cell.

To gain further insight in the degradation mechanisms of the latter device, the natural logarithm of the normalized FFs are shown in Fig. 5a for the three inverted devices. We observe that

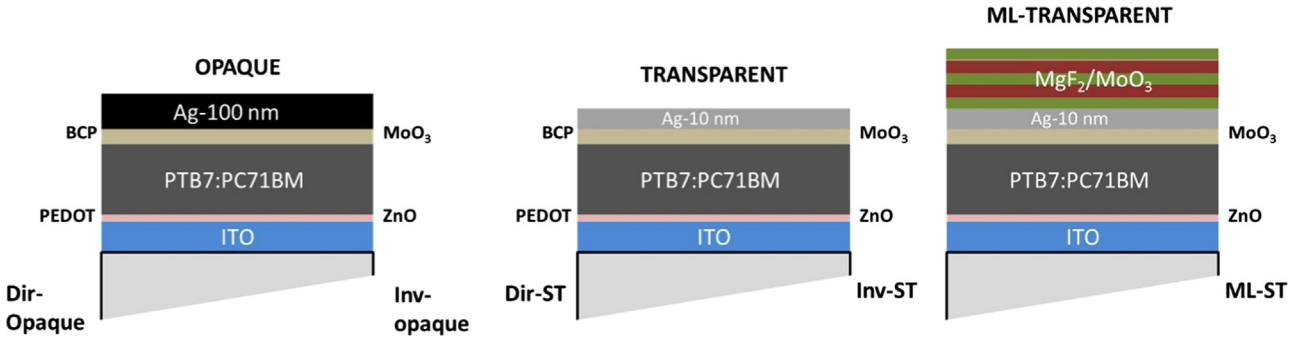

Fig. 1. Architecture for the OPV devices reported in this work. In all cases illumination was from the substrate side. The opaque samples differ from the transparent ones in the thickness of the Ag back-contact electrode. The blocking layers corresponding to standard and inverted solar cells architectures are indicated on the left and right of the drawings, respectively. Layer thicknesses are not drawn at scale.

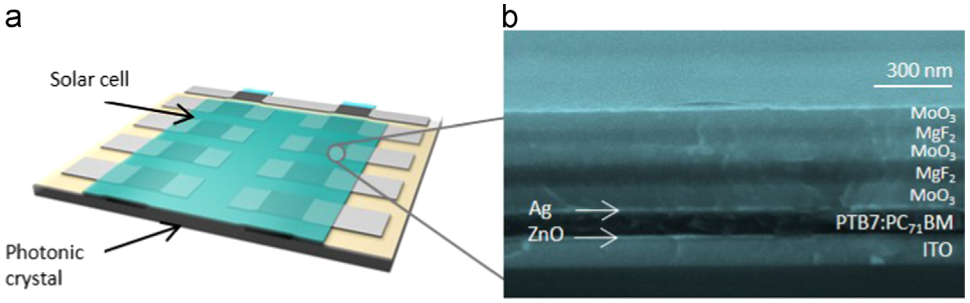

Fig. 2. Schematic and FESEM image of ML-ST. (A) Photovoltaic cells were fabricated on top of fused silica glass substrate. The cell area, i.e. the area over which the Ag and ITO electrodes overlap was 0.09 cm^3. The multilayer photonic structure was deposited on top of the electrical structure saving the silver contacts. (B) SEM cross-sectional micrograph of the ML-ST. The photovoltaic structure consists of two parts. On the one hand the electrical part based on PTB7:PCBM-based cell. On the other hand, the multilayered MoO_3/MgF_2 PC. In this particular case instead of on a glass substrate, the structure was grown on a doped-silicon substrate to avoid charging effects during the SEM scanning.

Table 2
PV parameters for five different configurations.

	J_{sc} (mA/cm^2)	V_{oc} (mV)	*FF*	Efficiency (%)	LUMINOSITY (%)
Std-Opaque	13.06	714	69	6.43	0
Std-ST	8.31	722	70	4.19	32
Inv-Opaque	13.26	746	73	7.27	0
Inv-ST	8.09	732	74	4.39	31.6
Inv-ML-ST	10.02	745	72	5.37	30.1

for the Inv-ML-ST cell, after an initial transient of approximately 1000 h, the FF experiences a slow exponential decay with a decay time of 10,500 h. The degradation in performance for the Inv-ST cell exhibits, first, a fast exponential decay up to approximately 1000 h, and second, a very slow decay time once the cell is already practically useless. The Inv-Opaque exhibits a similar behavior but delayed 500 h. In such first 500 h the evolution of such opaque cell is similar to the long exponential decay of the Inv-ML-ST cell. As can be seen in Fig. 5a, such long decay observed for the Inv-ML-ST cell can be adjusted to one single exponential, indicating one dominant mechanism of degradation for such devices. By comparing the decay rates for the three different type of devices, shown in Fig. 5a, we observe that a larger cell isolation can be associated to a larger cell lifetime indicating that degradation may be linked to the external agents such as oxygen and moisture.

We monitored the evolution the R_s and R_{sh} for the three devices under study shown in Fig. 5b and c, respectively. For the Inv-ML-ST device the R_s exhibits a slow increase over time while the R_{sh} degrades faster except for an initial period where that resistance increased slightly. A degradation of the device dominated by the R_{sh} over the R_s is an indication that such degradation is primarily located in the active material. For the Inv-Opaque the thick Ag metal electrode also serves as a barrier to protect the active part, but in this case the barrier is thinner and, once the corrosive agents reach effectively the active layer, the degradation becomes very rapid. For the Inv-ST, the lack of any protection barrier leads to an almost immediate degradation of both, the R_s and R_{sh}.

Additional information from the degradation mechanism can be obtained by measuring the time evolution of impedance on an Inv-Opaque cell at different voltages. Impedance experimental data have been fitted with the equivalent circuit shown in the inset of Fig. 6a in accordance with the model described in Refs. [23–25]. It consists of a series resistance, R_S, modelling metallic contacts, wires, etc., and a parallel resistance, R_P, that accounts for the cell dynamical resistance. The circuit also includes a constant phase element (CPE) that is a non-ideal capacitance taking into account non-homogeneities such as porosities, roughness and surface states and it presents an impedance given by $Z_{CPE} = 1/(CPE_T)(j\omega)^{(CPE_P)}$ with CPE_P ranging from 0 to 1 and CPE_T being approximately the capacitance value (when $CPE_P=1$). Finally, the circuit includes a Warburg element that models the existence of slowly diffusion charges, typically ions with an associated impedance given by $W = R_W \tanh (j\omega C_T)^{C_P}/(j\omega C_T)^{C_P}$ where R_W is the Warburg resistance associated to the size of the low frequency tail in the Nyquist plot, C_T is a coefficient related to diffusion effects and C_P is related to roughness of the diffusion media [26]. For $V < 0.6$ V the Warburg feature is not observed and therefore R_w is set to 0.

Nyquist plots at four different voltages are shown in Fig. 6 as examples of impedance measurements for three different times. We observe a good agreement between the experimental data and the theoretical fit. The main feature in the complex plane is a typical depressed semicircle in the medium-high frequency range, a standard behaviour in organic solar cells associated to carrier recombination. The semicircle diameter increases with time, which implies an increase of the parallel resistance R_P. This leads to a

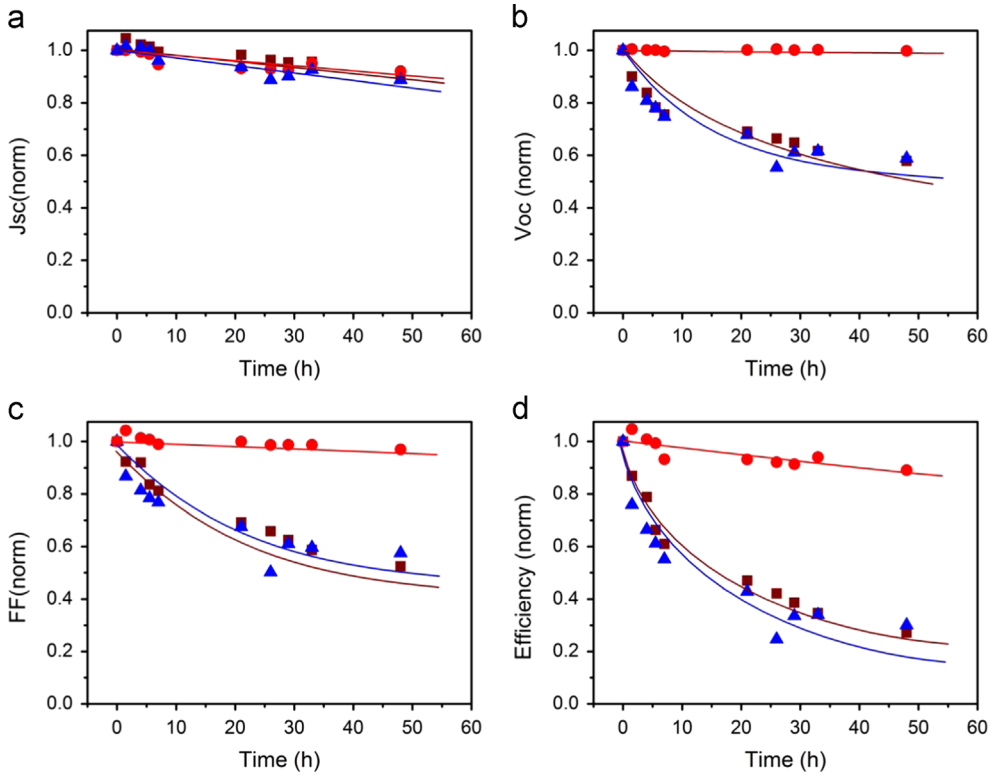

Fig. 3. Evolution of the PV parameters for Std-Opaque (Wine squares), Std-ST (Blue triangles), and Inv-ST (red circles) solar cells. All parameters are normalized to their respective value at $t=0$ h. The lines are guides for the eye. (For interpretation of the references to color in this figure legend, the reader is referred to the web version of this article.)

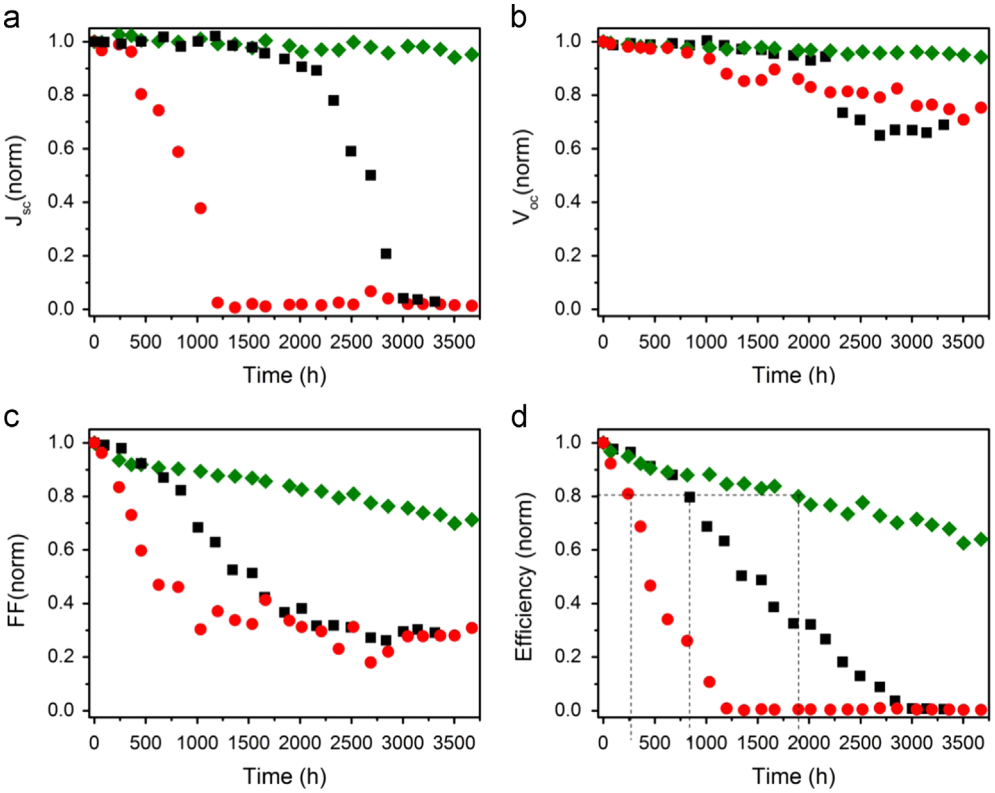

Fig. 4. Evolution of the normalized PV parameters for Inv-Opaque (black squares), Inv-ST (red circles) and ML-ST (green diamonds) cells: J_{sc} (a), V_{oc} (b), FF (c), and Eff (d) All parameters are normalized to the respective value at $t=0$ h. The dotted lines in (d) indicate the time at which the efficiency is 80% of the initial value. The life-times of the Inv-ST/Inv-Opaque/MS-ST cells were approximately 250/750/1900 h. (For interpretation of the references to color in this figure legend, the reader is referred to the web version of this article.)

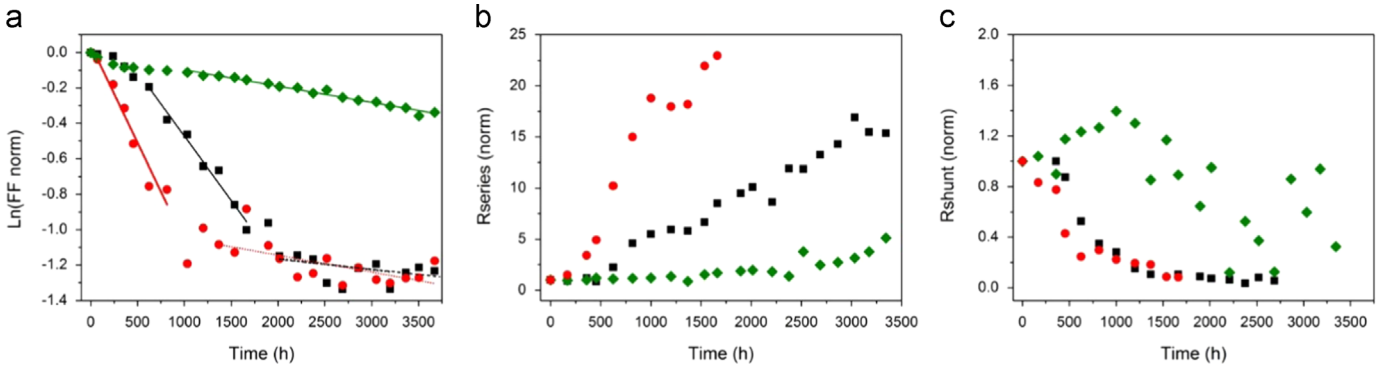

Fig. 5. Evolution of the (a) natural logarithm of the cell FF, (b) the series resistance and, (c) the shunt resistance for Inv-Opaque (black squares), Inv-ML-ST (green diamond), and Inv-ST (red circles) solar cells. (For interpretation of the references to color in this figure legend, the reader is referred to the web version of this article.)

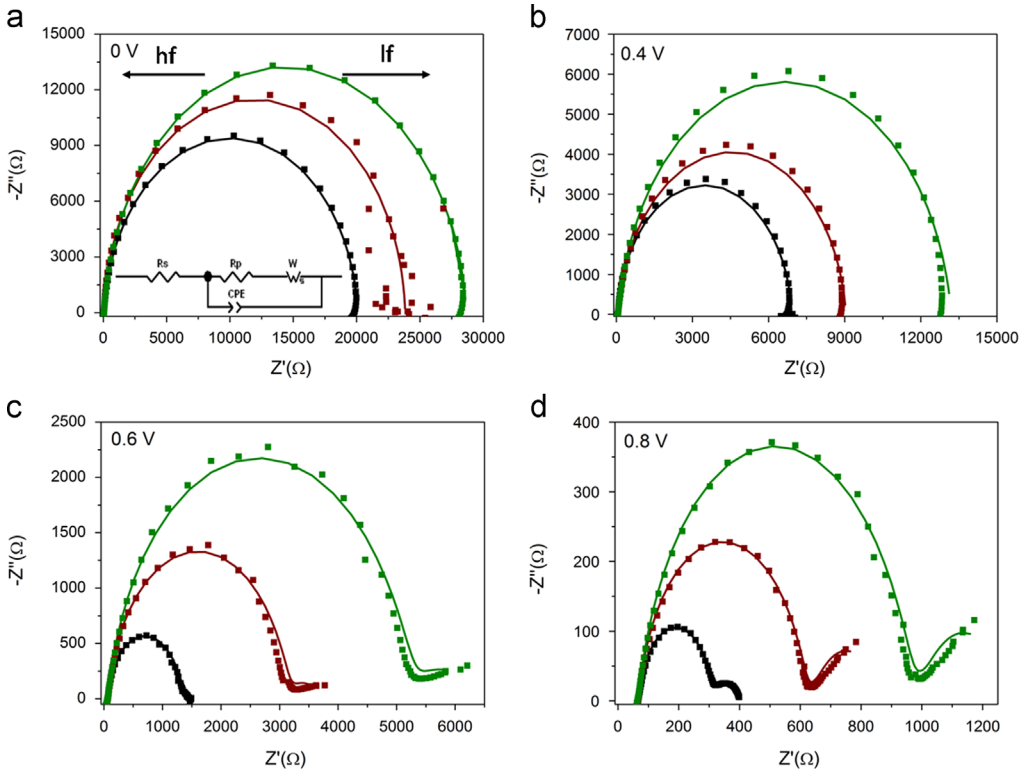

Fig. 6. Impedance spectra of the Inv-Opaque cell measured at (a) 0 V (b) 0.4 V (c) 0.6 V and (d) 0.8 V, and at three different times (solid squares). Solid lines correspond to the theoretical fit. Inset in (a) corresponds to the equivalent circuit scheme used to fit the experimental data.

corresponding rise of the recombination time and therefore to an enhancement of the carrier density. Besides, the semicircle depression is more pronounced with time, leading to a decrease of CPE_P parameter, and thus moving away from the ideal capacitor behaviour. At low frequencies, for $V=0.6$ and 0.8 V, one may observe a tail associated to a Warburg behaviour that is more pronounced as time evolves. This results in an increase of the Warburg resistance, obtaining values of $R_W=148.3$ (98.6) Ω at $t=0$, $R_W=447.6$ (237.8) Ω at $t=1176$ h and $R_W=683$ (311) Ω at $t=2232$ h for $V=0.6$ (0.8) V. The increase in R_W suggests an increment in the number of slowly moving charges as the cell degrades attributed to the heavy ions that are being dragged into the active blend by the water that penetrates in the cell as times evolves. This result would be in agreement with a cell degradation dominated by a rapid decrease in the shunt resistance for the opaque cell as we observed in Fig. 5c. It is observed that R_w is higher for 0.6 V than for 0.8 V. This could appear bizarre at first glance. However, this should be analysed in comparison with the recombination resistance R_p. The ion diffusion process modelled by R_w cannot be analysed by itself, but always related to the recombination mechanism. In fact, it is the ratio R_w/R_p that gives an idea of the ion diffusion influence on the overall dynamical process. This ratio increases with voltage, being for the last day of measurement 0.18 and 0.24 for 0.6 V and 0.8 V, respectively. This result suggests that ion diffusion is linked to carrier recombination, as R_p increases, carrier recombination decreases enhancing carrier density and hindering ion diffusion.

When inverted configuration devices are sealed, penetration of moisture is prevented and the cells exhibit a decay time constant close to 2000 h. We performed ISOS-L-3 tests and observed, as shown in Fig. 1S a of the Supplementary data file, that the FF of inverted devices exhibits a two exponential type degradation being the time constant of the rapid one 14 h and 1960 h for the slow one. When the UV light from the solar simulator is filtered using a GG400 filter, the rapid degradation disappears and, as shown in Fig. 1Sb of the Supplementary data file, the FF of the cell degrades following an almost single exponential decay with a time constant above 2000 h.

4. Conclusions

We have considered the over time performance of five different PTB7:$PC_{71}BM$ cell configurations and concluded that for unsealed devices when isolation from external corrosive elements increases, the degradation becomes clearly dominated by the sole action of such external agents. In such conditions degradation can be directly linked to a decrease in the shunt resistance. Additionally, we performed an impedance study that suggested an increase in the presence of slowly moving charges as the degradation of the cell developed. The partial but rather effective cell isolation we implemented was achieved by the deposition of five layers of dielectrics with a total thickness of 554 nm. Lifetimes for inverted semi-transparent cells including such layer stack were close to 8 times the lifetime for equivalent cells without the stack and 400 times larger when compared to standard configuration semi-transparent cells. When comparing semi-transparent devices to opaque ones, the reduced thickness of the metal electrode did not seem to have a direct effect on the cell lifetime other than being a less effective barrier to external corrosive agents. For sealed devices where further penetration of such corrosive elements is prevented, degradation appears to be dominated by a photo-degradation that can be slowed down when UV light is filtered out. The time evolution results we reported for cells fabricated with the PTB7:PC71BM blend, clearly indicate that such cells have the potential to become stable in the event that the fabricated devices are properly isolated from the surrounding environment.

Acknowledgements

This work was supported by the Ministerio de Economía y Competitividad with the grants MAT2011-28665, IPT-120000-2010-29 and IPT-2012-0986-120000, and we acknowledge support from the EC under the project Solprocel with grant number no. 604506.

Appendix A. Supporting information

Supplementary data associated with this article can be found in the online version at http://dx.doi.org/10.1016/j.solmat.2015.01.026.

References

[1] L. Lu, L. Yu, Understanding low bandgap polymer PTB7 and optimizing polymer solar cells based on it, Adv. Mater. 26 (26) (2014) 4413.
[2] Y. Liang, Z. Xu, J. Xia, S.T. Tsai, Y. Wu, G. Li, C. Ray, L. Yu, For the bright future—bulk heterojunction polymer solar cells with power conversion efficiency of 7.4%, Adv. Mater. 22 (20) (2010) 135.
[3] R. Betancur, P. Romero-Gomez, A. Martinez-Otero, X. Elias, M. Maymo, J. Martorel, Nat. Photonics 7 (12) (2013) 995.
[4] M. Jørgensen, K. Norrman, S.A. Gevorgyan, T. Tromholt, B. Andreasen, F.C. Krebs, Stability of polymer solar cells, Adv. Mater. 24 (5) (2012) 580.
[5] C.H. Peters, I.T. Sachs-Quintana, J.P. Kastrop, S. Beaupre, M. Leclerc, M.D. McGehee, High efficiency polymer solar cells with long operating lifetimes, Adv. Energy Mater. 1 (2011) 491.
[6] D. Angmo, S.A. Gevorgyan, T.T. Larsen-Olsen, R.R. Søndergaard, M. Hösel, M. Jørgensen, R. Gupta, G.U. Kulkarni, F.C. Krebs, Scalability and stability of very thin, roll-to-roll processed, large area, indium-tin-oxide free polymer solar cell modules, Org. Electron. 14 (3) (2013) 984.
[7] T.Y. Chu, S.W. Tsang, J. Zhou, P.G. Verly, J. Lu, S. Beaupre, M. Leclerc, Y. Tao, High-efficiency inverted solar cells based on a low bandgap polymer with excellent air stability, Sol. Energy Mater. Sol. Cells 96 (1) (2012) 155.
[8] N. Espinosa, R. Garcıa-Valverde, A. Urbina, F.C. Krebs, A life cycle analysis of polymer solar cell modules prepared using roll-to-roll methods under ambient conditions, Sol. Energy Mater. Sol. Cells 95 (2011) 1293.
[9] S. Gunes, H. Neugebauer, N.S. Sariciftci, Conjugated polymer-based organic solar cells, Chem. Rev. 107 (4) (2007) 1324.
[10] S. Woo, W.H. Kim, H. Kim, Y. Yi, H.K. Lyu, Y. Kim, 8.9% Single-stack inverted polymer solar cells with electron-rich polymer nanolayer-modified inorganic electron-collecting buffer layers, Adv. Energy Mater. 4 (7) (2014) 1301692.
[11] Y. Sun, Ch.J. Takacs, S.R. Cowan, J. HwaSeo, X. Gong, A. Roy, A.J. Heeger, Efficient, air-stable bulk heterojunction polymer solar cells using MoO_x as the anode interfacial layer, Adv. Mater. 23 (19) (2011) 2226.
[12] M. Manceau, A. Rivaton, J-L. Gardette, S Guillerez, N. Lemaître, The mechanism of photo- and thermooxidation of poly(3-hexylthiophene) (P3HT) reconsidered, Polym. Degrad. Stab. 94 (6) (2009) 898.
[13] R. Grisorio, G. Allegretta, P. Mastrorilli, G.P. Suranna, On the degradation process involving polyfluorenes and the factors governing their spectral stability, Macromolecules 44 (20) (2011) 7977.
[14] P.C. Yang, J.Y. Sun, S.Y. Ma, Y.M. Shen, Y.H. Lin, C.P. Chen, C.F. Lin, Interface modification of a highly air-stable polymer solar cell, Sol. Energy Mater. Sol. Cells 98 (2012) 351.
[15] Z. He, C. Zhong, S. Su, M. Xu, H. Wu, Y. Cao, Enhanced power-conversion efficiency in polymer solar cells using an inverted device structure, Nat. Photonics 6 (9) (2012) 591.
[16] Z. Lin, C. Jiang, C. Zhu, J. Zhang, Development of inverted organic solar cells with TiO_2 interface layer by using low-temperature atomic layer deposition, Appl. Mater. Interfaces 5 (3) (2013) 713.
[17] A. Martínez-Otero, X. Elias, R. Betancur, J. Martorell, High-performance polymer solar cells using an optically enhanced architecture, Adv. Opt. Mater. 1 (1) (2013) 37.
[18] Y. Sun, J.H. Seo, C.J. Takacs, J. Seifter, A.J. Heeger, Polymer bulk heterojunction solar cells: function and utility of inserting a hole transport and electron blocking layer into the device structure, Adv. Mater. 23 (14) (2011) 1679.
[19] N.P. Sergeant, A. Hadipour, B. Niesen, D. Cheyns, P. Heremans, P. Peumans, B.P. Rand, Adv. Mater. 24 (6) (2012) 728.
[20] R. Betancur, A. Martinez-Otero, X. Elias, P. Romero-Gomez, S. Colodrero, H. Miguez, J. Martorell, Optical interference for the matching of the external and internal quantum efficiencies in organic photovoltaic cells, Sol. Energy Mater. Sol. Cells 104 (2012) 87.
[21] M.O. Reese, et al., Consensus stability testing protocols for organic photovoltaic materials and devices, Sol. Energy Mater. Sol. Cells 95 (2011) 1253–1267.
[22] M.P. de Jong, L.J. van IJzendoorn, M.J.A. de Voigt, Stability of the interface between indium-tin-oxide and poly(3,4-ethylenedioxythiophene)/poly(styrenesulfonate) in polymer light-emitting diodes, Appl. Phys. Lett. 77 (2000) 2255.
[23] Xinhong Peng, Hongbing Yu, Xin Wang, Ningshengjie Gao, Lijuan Geng, Lina Ai, Enhanced anode performance of microbial fuel cells by adding nanosemicondutor goethite, J. Power Sources 223 (2013) 94–99.
[24] Yanming Zhao Youzhong Dong, He Duan, Zhiyong Liang, Enhanced electrochemical performance of $LiMnPO_4$ by Li^+ conductive Li_3VO_4 surface coatinns, Electrochim. Acta 123 (2014) 244–250.
[25] Zhuguo Li Ruifeng Li, Yanyan Zhu, Kai Qi, Structure and corrosion resistance properties of Ni–Fe–B–Si–Nb amorphous composite coatings fabricated by laser processing, J. Alloys Compd. 580 (2013) 327–331.
[26] C. Lopez-Lopez, S. Colodrero, S.R. Raga, H. Lindstrom, F. Fabregat-Santiago, J. Bisquert, H. Miguez, J. Mater. Chem. 22 (5) (2012) 1751.